TNO PUBLIEK



Westerduinweg 3 1755 LE Petten P.O. Box 15 1755 ZG Petten The Netherlands

www.tno.nl

T +31 88 866 50 65

TNO report

TNO 2019 R10059 | Final report

Validation at High Frequency of Wind Field
Reconstruction from Scanning Lidar using
Gaussian Processes

Date 22 January 2018

Author(s) C.F.W. Stock-Williams

G. Bergman J. Duncan

Copy no No. of copies

Number of pages 19 (incl. appendices)

Number of appendices Sponsor

Project name Innovation 2018 -- Machine Learning and Scanning Lidar

Project number 5.5263.01.17.01

All rights reserved.

No part of this publication may be reproduced and/or published by print, photoprint, microfilm or any other means without the previous written consent of TNO.

In case this report was drafted on instructions, the rights and obligations of contracting parties are subject to either the General Terms and Conditions for commissions to TNO, or the relevant agreement concluded between the contracting parties. Submitting the report for inspection to parties who have a direct interest is permitted.

© 2018 TNO

Summary

During 2017, a novel method was developed – based on a machine learning approach called Gaussian Process Regression – for using raw Lidar data to reconstruct instantaneous 3D wind fields. This method was successfully validated using a Windcube v2 ground-mounted static beam Lidar, against 10-minute averaged data from several cup anemometers at different heights on a met mast located on a site with "simple" terrain.

The current report summarises an innovation project funded by ECN part of TNO to collect a new data set using its Windcube 200s scanning Lidar, in order to:

- 1 validate against a 3D sonic anemometer at 1Hz frequency for clean and complex wind conditions;
- 2 understand how the method performs when applied to a different Lidar design and scanning pattern.

Apart from implementing a method to filter laser pulse reflections from the met mast, no changes were required to the method presented in previous reports.

Four scanning patterns were tested, altering the speed and azimuthal scanning range. The beam-resolved wind speed predicted by the machine learning method is validated against the wind velocity measured by the sonic anemometer, resolved to the angle from the Lidar to the sonic anemometer; the results are shown in Table 1.

Validation test	Length of test (days)	Bias (m/s)	Scatter (m/s)
Fast-Narrow	3	0.07	0.78
Fast-Wide	6	0.20	0.61
Slow-Narrow	10	-0.06	0.56
Slow-Wido	25	-0.05	0.01

0.03

0.40

Table 1 Results of validation analyses against a sonic anemometer.

30

These results indicate that scanning Lidar measurements, processed through Gaussian Process reconstruction methods, can be used to reproduce reliable 1Hz measurements. The conditions experienced at the EWTW site are complex, both in terms of atmospheric physics, but also the wakes from a very large number of turbines. No filters have been applied on the results by wind direction or wind speed. After all, the intention is to create a method that works in all wind conditions.

There are some limitations, in particular, it appears that no matter what scanning pattern is used, turbulence with a timescale below 10 seconds is unlikely to be resolved. For comparison, with the static WindCube v2, turbulent features down to about 3 seconds were observed. This may be caused by the characteristics of the Lidar scanning pattern, or the Gaussian Process analysis, or a combination of both.

This study has identified further work:

Cup anemometer

- 1 an error in the code has been identified which causes some errors at the boundaries between hours; which should be fixed.
- 2 the conversion of Lidar beam speed to wind velocity remains an open question, although some work has been completed on algorithms intended to solve this.

Contents

	Summary	
1	Introduction	4
2	Data Set	5
2.1	Instrument Locations	5
2.2	Lidar	
2.3	Sonic Anemometer	6
2.4	Timeline	7
3	Updates to Analysis Method	8
4	Results	g
4.1	Data Processing	g
4.2	Fast-Narrow	
4.3	Fast-Wide	
4.4	Slow-Narrow	
4.5	Slow-Wide	
5	Analysis and Conclusions	17
6	References	19

1 Introduction

During 2017, a novel method was developed – based on a machine learning approach called Gaussian Process Regression – for using raw Lidar data to reconstruct instantaneous 3D wind fields.

As described in the final report [1] and subsequent paper [2], data from Windcube v2 ground-mounted static beam Lidar units (supplied by Leosphere) were used for development. The results were validated against 10-minute averaged data from several cup anemometers at different heights on a met mast located on a site with "simple" terrain.

In that project, it was not possible to finish exploring some important questions:

- 1. Establishing and implementing a good method for reconstructing the wind velocity from the radial speeds output by the Gaussian Processes.
- 2. Fully validating the methodology, by comparison at high frequency (at least 1 Hz) against 3D velocity measurements.
- 3. Understanding how the method performs using other Lidar machines and data acquisition geometries.

In 2018, therefore, ECN part of TNO funded an internal innovation project to collect a new data set and run analysis sufficient to answer the second and third open questions above. In the event of successful results, this brings the method closer to certification for commercial use.

2 Data Set

2.1 Instrument Locations

A scanning lidar (see section 2.2) was installed on the ECN Wind turbine Test site Wieringermeer (EWTW), next to one of the prototype turbines, as indicated in Figure 1.



Figure 1 Satellite image from Google Earth showing the layout of the wind turbine test site Wieringermeer. The lidar is indicated by the square next to turbine labelled PW7. The met mast with the sonic anemometer is indicated by the triangle labelled M6.

A sonic anemometer (see section 2.3) is placed on a met mast 123m above ground level and at an angle of 140 degrees on a 3m boom. Figure 2 shows the placement of the sonic anemometer on the met mast. Above it (at 127m) on the same boom, there is a Thies Wind Transmitter First Class Advanced cup anemometer.

The location of the scanning lidar was 52.818943 N, 5.055757 E (638531m N 5854110m E in UTM co-ordinates). According to [4], the met mast is located at 52.816613 N, 5.051749 E (638268m N 5853843m E).

From this information, the vector from the lidar to the sonic anemometer should be [-261,-269,123].

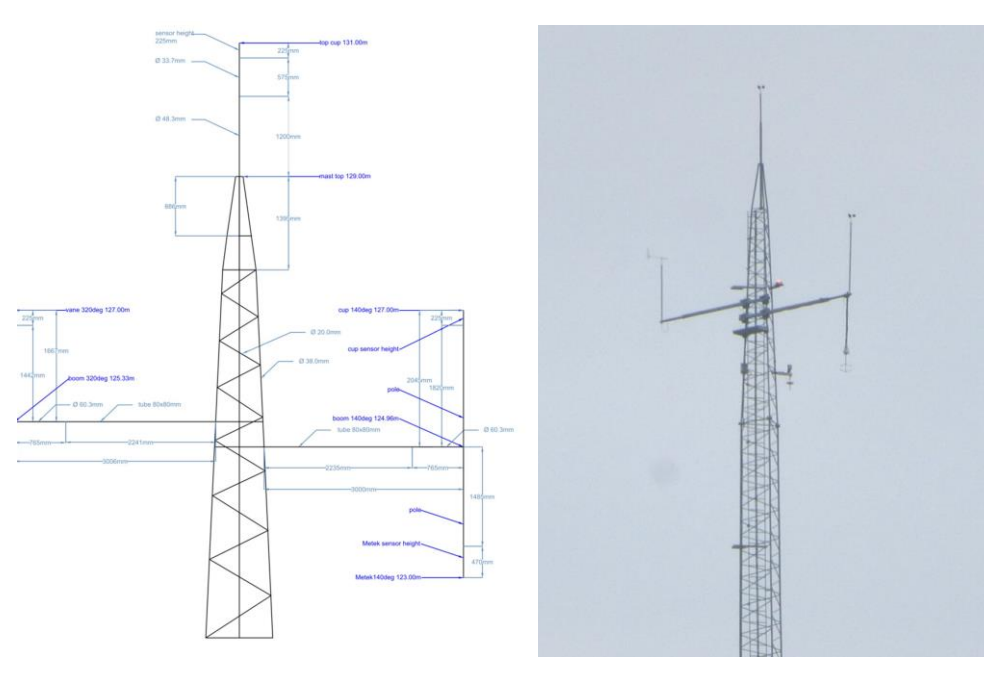


Figure 2 Arrangement of the top of the MM6 met mast – showing the sonic anemometer installed upside-down on the 127m, 140 degree boom.

2.2 Lidar

ECN part of TNO owns a Leosphere Windcube 200s scanning lidar unit. The specifications can be found online at [3].

The lidar can be set up in a few different scanning regimes. The PPI mode was chosen, with the following properties:

- 9 range gates: from 270m to 510m in 30m steps.
- 2 degree azimuthal resolution.
- Azimuthal range centred at 226.5 degrees (the azimuthal angle from the lidar to the met mast).
- 4 elevation steps: 10, 14, 18 and 22 degrees (the elevation angle from the lidar to the sonic anemometer is approximately 16 degrees).

Four different scanning patterns were chosen, in order to investigate the impact of spatial and temporal separation of the input data on the uncertainty and accuracy of the wind reconstruction. These were constructed from all combinations of:

Speed

"Slow": 5 degrees/s "Fast": 20 degrees/sAzimuthal Scanning Range

"Wide": 30 degrees "Narrow": 10 degrees

2.3 Sonic Anemometer

The instrument used for validation is a Metek uSonic-3, whose specifications and calibration certificate are provided in [4] and online at [5]. It measures temperature and the three components of wind velocity.

In order to obtain wind direction as a rotation clockwise from North at 0° , it is necessary to first rotate the measured horizontal direction θ (calculated from the horizontal u and v components of the wind velocity) clockwise by 128.254°, before inverting the sense of rotation by calculating (270° - θ).

2.4 Timeline

The timeline of the experimental data collection is given in Table 2.

Table 2 Timeline of data collection and different scanning patterns.

Scanning pattern	Start of data collection	End of data collection
Fast-Narrow	2018-05-25 13:15 UTC	2018-05-28 12:47 UTC
Fast-Wide	2018-05-29 11:15 UTC	2018-06-04 06:00 UTC
Slow-Narrow	2018-06-04 06:04 UTC	2018-06-14 13:15 UTC
Slow-Wide	2018-06-14 13:22 UTC	2018-07-09 11:00 UTC

3 Updates to Analysis Method

A new parsing program needed to be written to load and re-format the scanning Lidar raw data files, and save out data in 1-hour blocks.

After some experimentation, it was realised that the met mast structure reflected some of the Lidar pulses, causing systematic errors in the data over a large area around the structure. As a result the following additional quality check was implemented:

- 1. Load in each raw Lidar data file.
- 2. Calculate the mean and standard deviation of the Carrier-to-Noise-Ratio (CNR).
- 3. Rescale the CNR values into a z score: $z = \frac{(CNR Mean)}{Std. Deviation}$
- 4. Flag all data points with a z score *greater than* 2.5. This removes all points with an unnaturally-large signal: which is likely to have come from reflection off a hard surface, rather than backscatter from atmospheric aerosols.

This needs to be done separately for each file, rather than fixing a single CNR threshold, because the intrinsic backscatter strength of the atmosphere varies with time.

Otherwise, no changes were required to the structure or assumptions built into the Gaussian Processes (GPs) described in [1] and [2].

4 Results

4.1 Data Processing

As with the previous study, the GP analysis enables instantaneous 3D mapping of the beam velocity from a "Virtual Lidar"; example 'slices' using the Lidar data are shown in Figure 3.

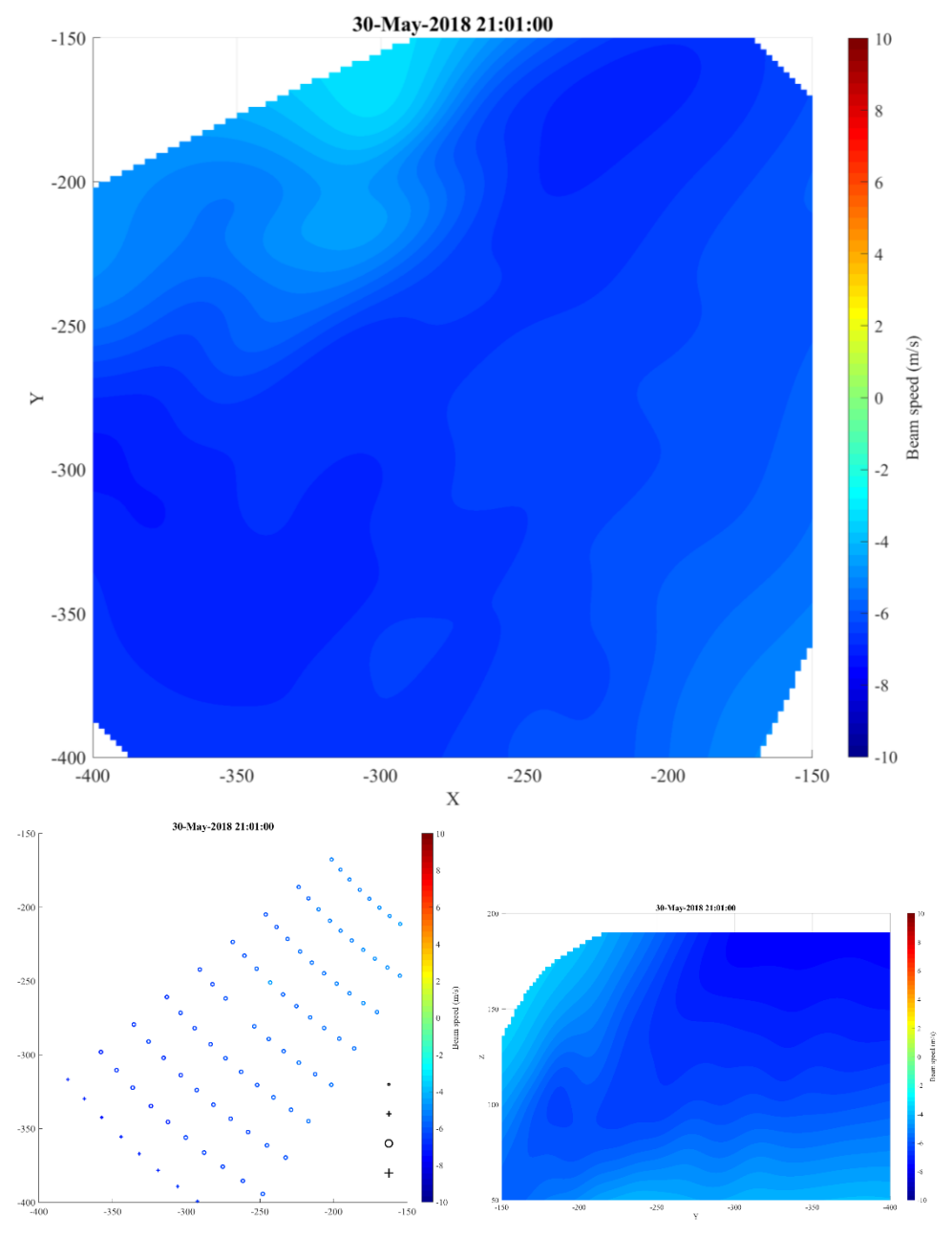


Figure 3 Top: Spatial map at 120m height above the ground of mean Lidar beam speed predicted by the Virtual Lidar at one instant in time, while the Lidar was in the fast-wide scanning pattern. Bottom, left: Plan view of data collected within one second of that time by the Lidar (size and shape of each point indicates its distance above [+] or below [o] the 120m plane). Bottom, right: Spatial map at X = -275m (west of the Lidar) of mean Lidar beam speed predicted by the Virtual Lidar at one instant in time.

The raw Lidar data were now processed to produce Lidar beam estimates at 1Hz at the location of the sonic anemometer: due to error in the calculations in section 2.1, the location required was actually [-272, -258, 123]; due to lack of time this issue could not be investigated fully and the results shown in this section assume the sonic anemometer is located at [-271, -259, 123] relative to the Lidar. Any predictions with an uncertainty standard deviation greater than 1m/s were removed.

The 4Hz data from the sonic anemometer were first averaged to 1Hz, and then resolved to the Lidar beam angle for direct comparison with the Lidar beam speeds predicted by the GP modelling.

For each scanning pattern, the internal Lidar clock appeared to shift (relative to the database clock referencing the sonic anemometer data). An automatic function was created to calculate and apply a time shift to best match the two time series.

The following sub-sections show results for each scanning pattern. The number of seconds shifted is displayed above each time series graph.

4.2 Fast-Narrow

Figure 4 gives an overview of the wind speeds (resolved to the Lidar beam) measured during the period and a comparison with the GP output.

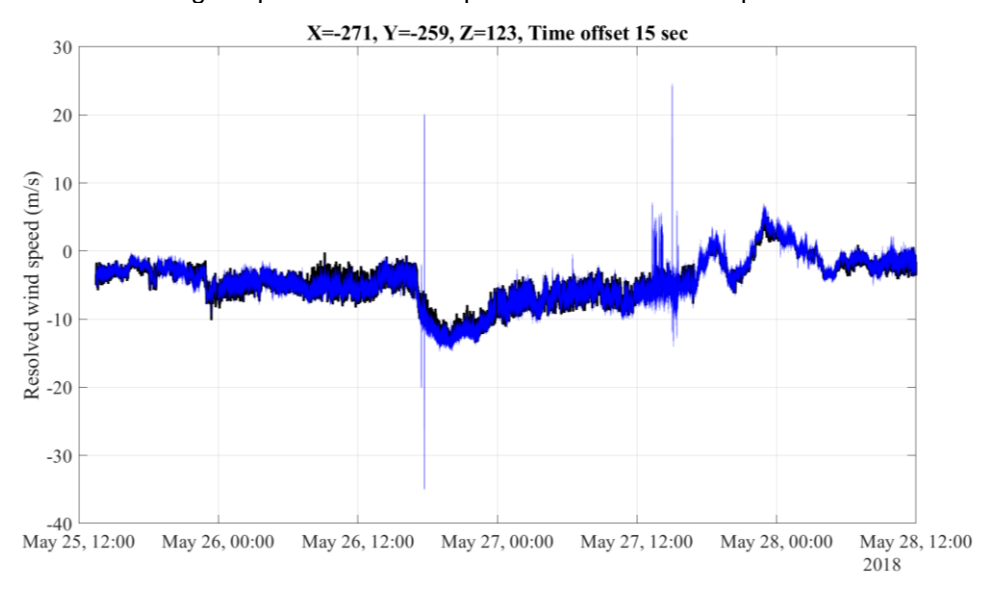


Figure 4 Comparison of sonic anemometer (black) with Lidar GP output (blue, including mean and +/- one standard deviation) while using the fast-narrow scanning pattern.

Figure 5 shows a close up of the agreement, for greater understanding.

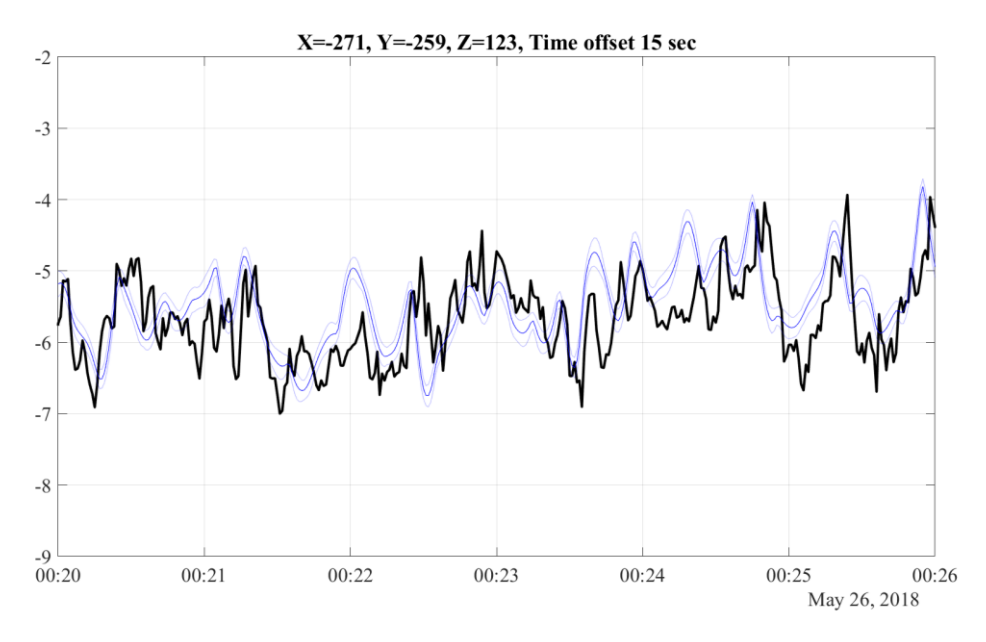


Figure 5 Six minutes of comparison of sonic anemometer (black) with Lidar GP output (blue, including mean and +/- one standard deviation) while using the fast-narrow scanning pattern.

Finally, validation can be effected by statistical calculations. The scatter plot is given in Figure 6, showing a bias of 0.069 (+/- 0.003) m/s and a scatter of [0.780, 0.784] m/s. 90% confidence intervals (assuming independence) are given.

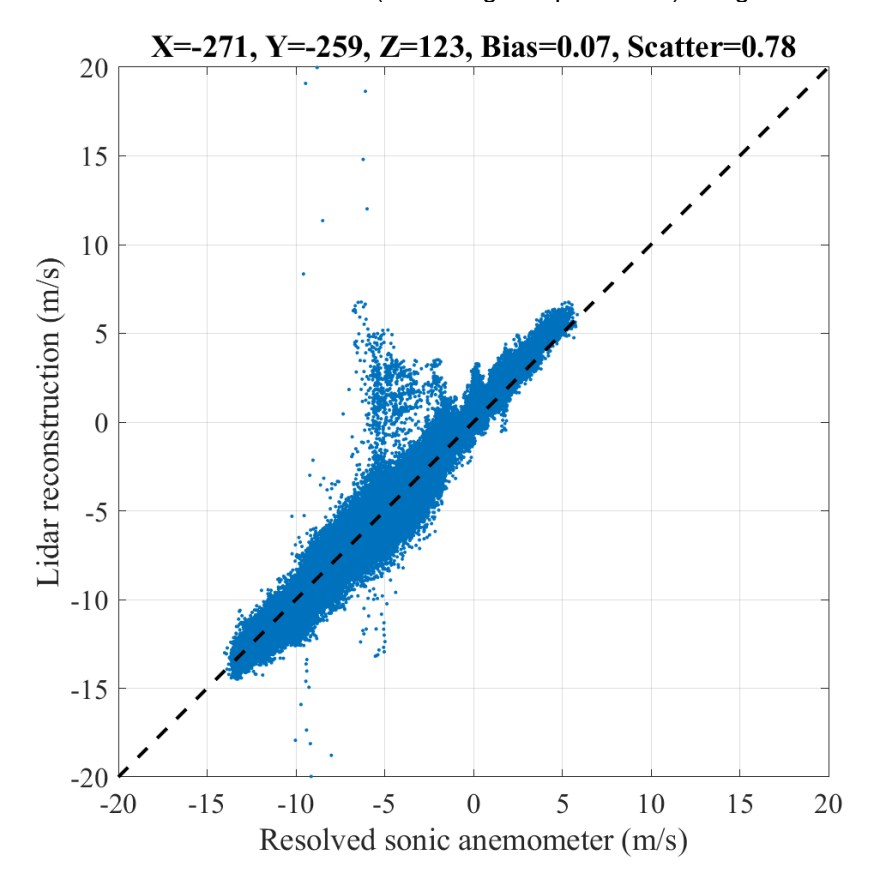


Figure 6 Scatter plot of resolved beam speeds from the GP reconstruction versus the sonic anemometer, while using the fast-narrow scanning pattern.

4.3 Fast-Wide

Figure 7 gives an overview of the wind speeds (resolved to the Lidar beam) measured during the period and a comparison with the GP output.

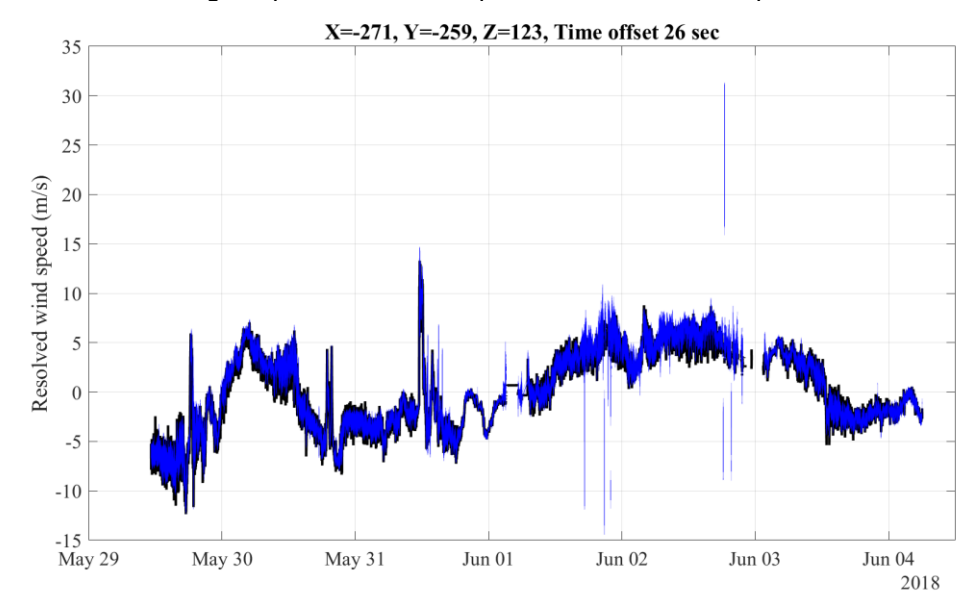


Figure 7 Comparison of sonic anemometer (black) with Lidar GP output (blue, including mean and +/- one standard deviation) while using the fast-wide scanning pattern.



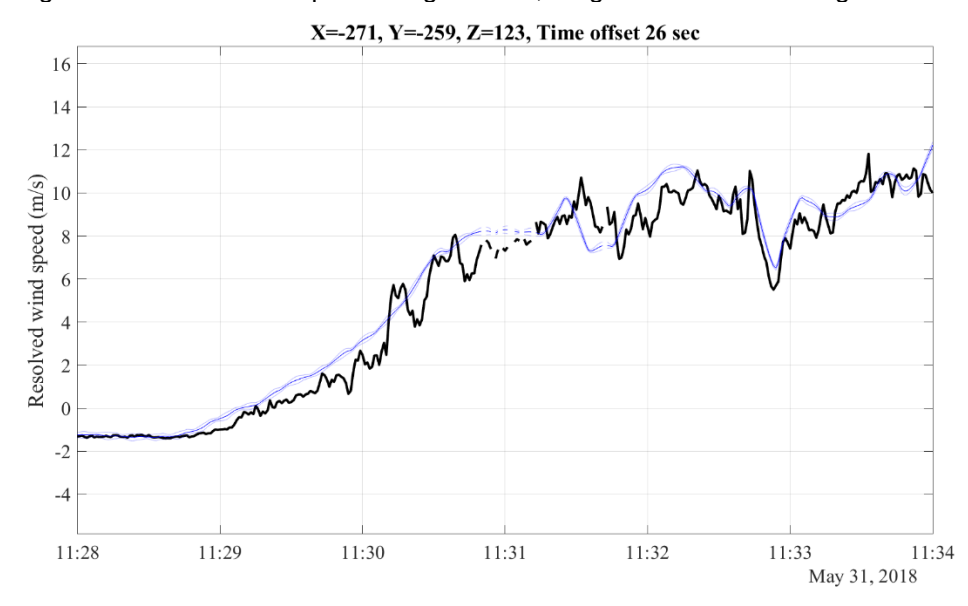


Figure 8 Six minutes of comparison of sonic anemometer (black) with Lidar GP output (blue, including mean and +/- one standard deviation) while using the fast-wide scanning pattern.

Finally, validation can be effected by statistical calculations. The scatter plot is given in Figure 9, showing a bias of 0.198 (+/- 0.001) m/s and a scatter of [0.606, 0.608] m/s. 90% confidence intervals (assuming independence) are given.

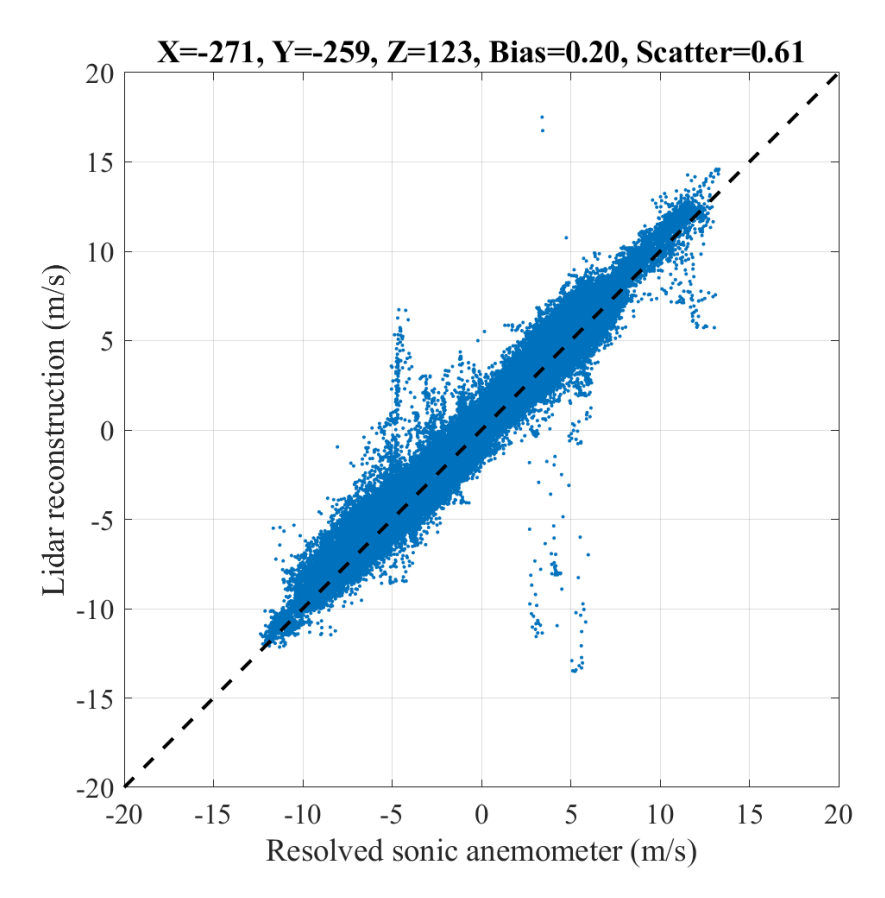


Figure 9 Scatter plot of resolved beam speeds from the GP reconstruction versus the sonic anemometer, while using the fast-wide scanning pattern.

4.4 Slow-Narrow

Figure 10 gives an overview of the wind speeds (resolved to the Lidar beam) measured during the period and a comparison with the GP output.

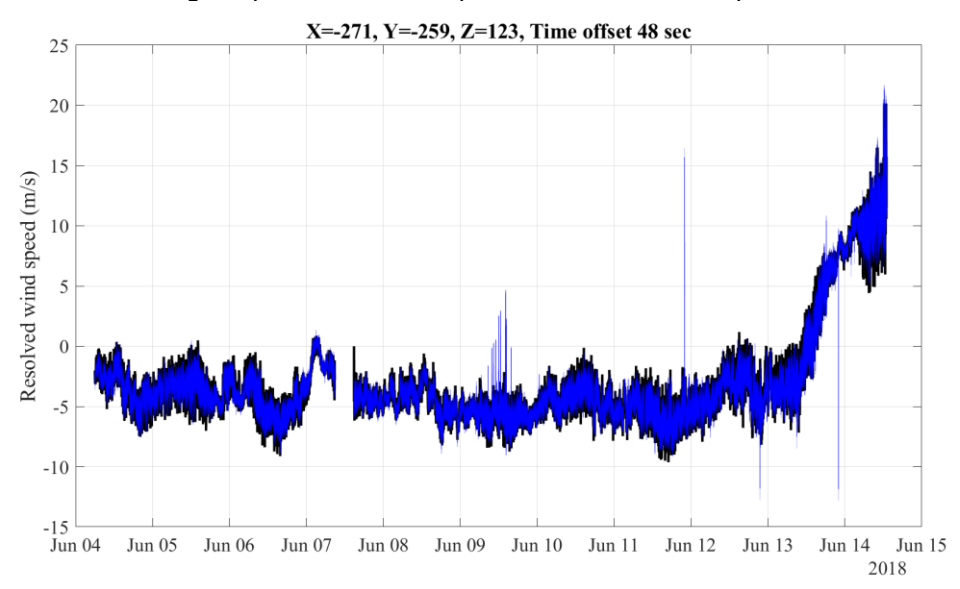


Figure 10 Comparison of sonic anemometer (black) with Lidar GP output (blue, including mean and +/- one standard deviation) while using the slow-narrow scanning pattern.

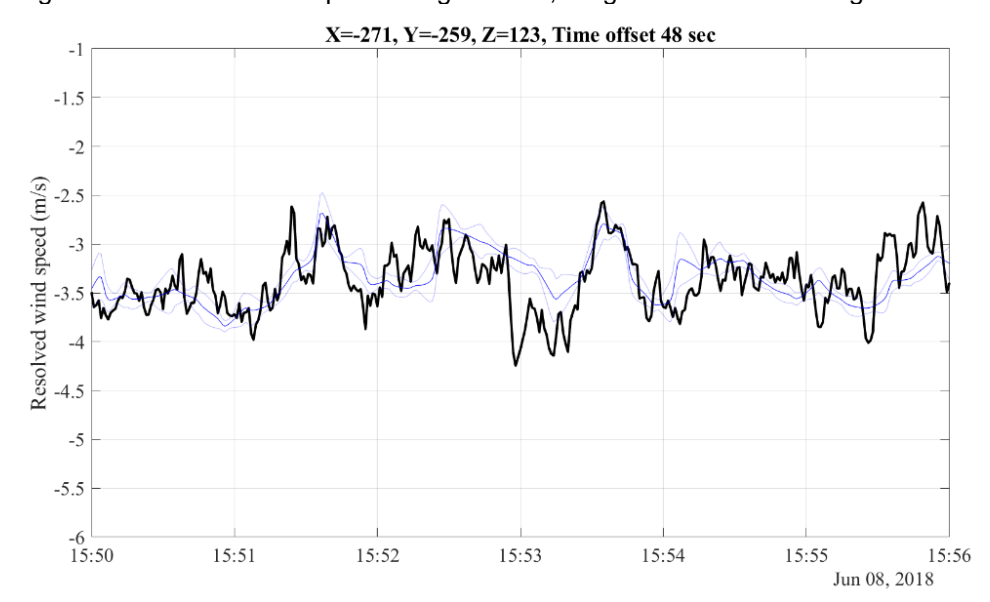


Figure 11 shows a close up of the agreement, for greater understanding.

Figure 11 Six minutes of comparison of sonic anemometer (black) with Lidar GP output (blue, including mean and +/- one standard deviation) while using the slow-narrow scanning pattern.

Finally, validation can be effected by statistical calculations. The scatter plot is given in Figure 12, showing a bias of -0.056 (+/- 0.001) m/s and a scatter of [0.558, 0.559] m/s. 90% confidence intervals (assuming independence) are given.

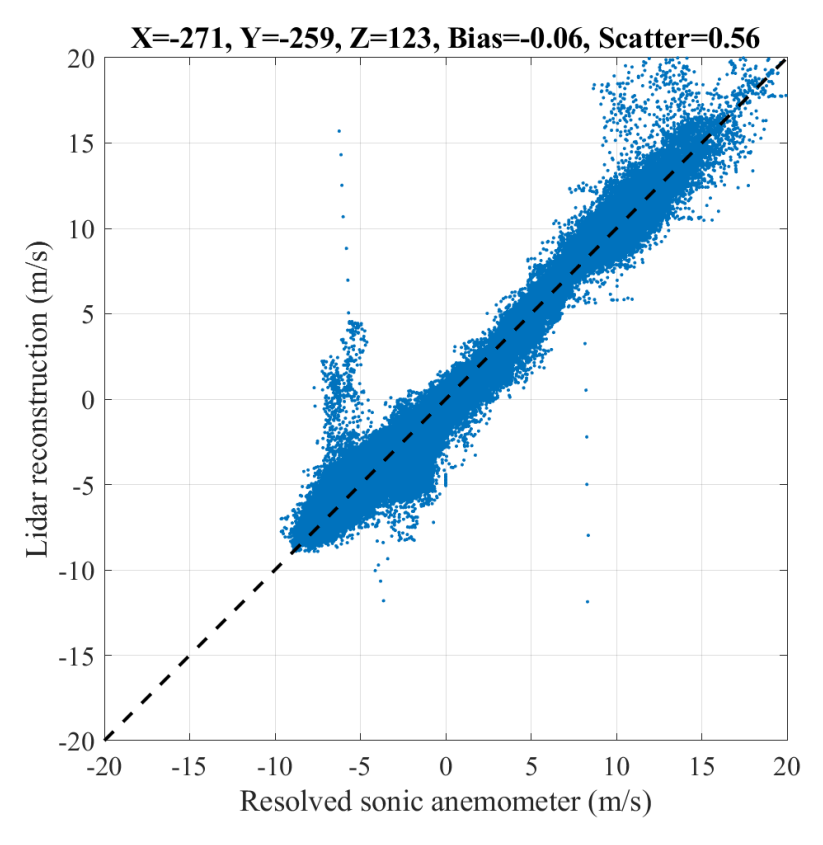


Figure 12 Scatter plot of resolved beam speeds from the GP reconstruction versus the sonic anemometer, while using the slow-narrow scanning pattern.

4.5 Slow-Wide

Figure 13 gives an overview of the wind speeds (resolved to the Lidar beam) measured during the period and a comparison with the GP output.

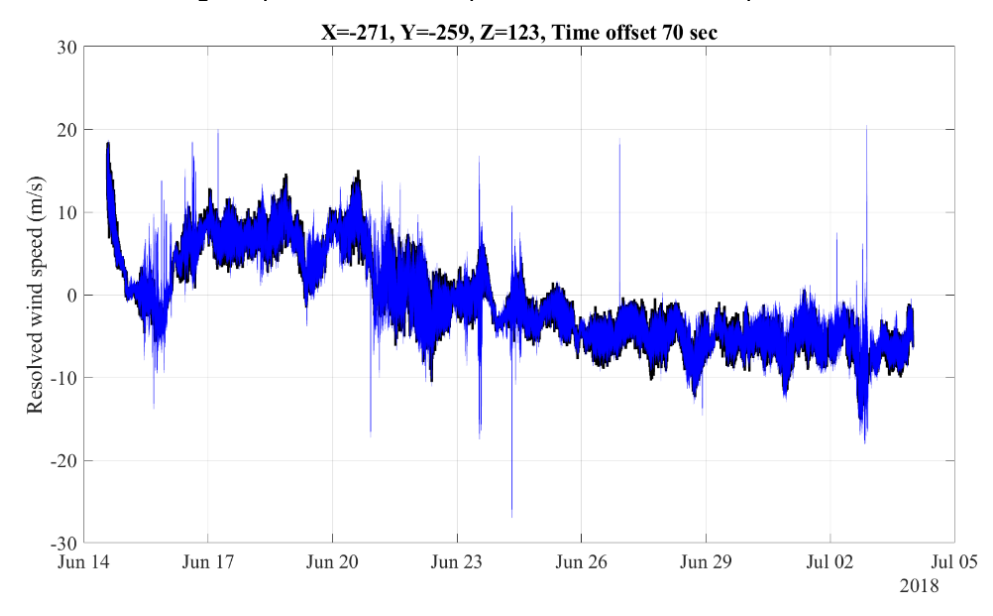


Figure 13 Comparison of sonic anemometer (black) with Lidar GP output (blue, including mean and +/- one standard deviation) while using the slow-wide scanning pattern.

Figure 14 shows a close up of the agreement, for greater understanding.

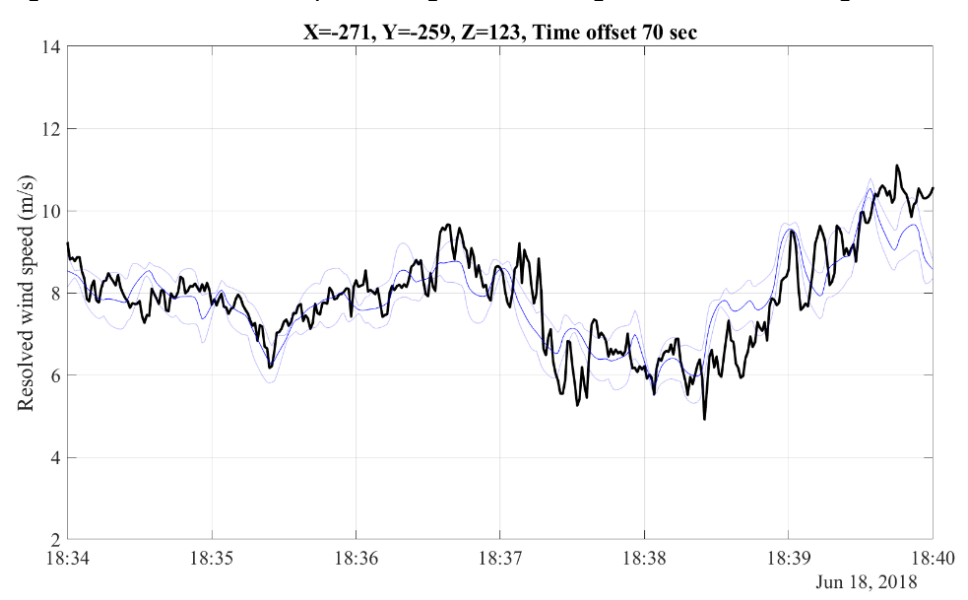


Figure 14 Six minutes of comparison of sonic anemometer (black) with Lidar GP output (blue, including mean and +/- one standard deviation) while using the slow-wide scanning pattern.

Finally, validation can be effected by statistical calculations. The scatter plot is given in Figure 15, showing a bias of -0.054 (+/- 0.001) m/s and a scatter of [0.908, 0.910] m/s. 90% confidence intervals (assuming independence) are given.

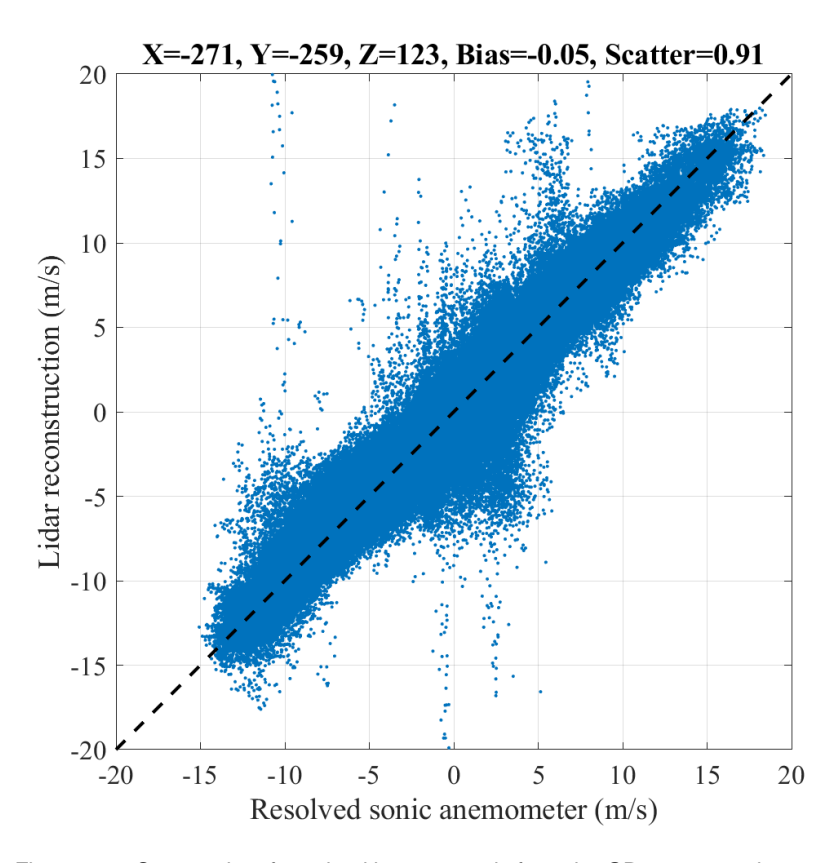


Figure 15 Scatter plot of resolved beam speeds from the GP reconstruction versus the sonic anemometer, while using the slow-wide scanning pattern.

5 Analysis and Conclusions

From the results presented in the previous section, it appears that Lidar measurements, processed through Gaussian Process reconstruction methods, can be used to reproduce reliable 1Hz measurements. The conditions experienced at the EWTW site are usually simple, but away from the dominant wind direction there are complex conditions, mostly due to wakes from a very large number of turbines, but also (at times of easterly or westerly winds) occasional complex shear profiles caused by lake-land-sea boundaries. No filters have been applied on the results by wind direction or wind speed. After all, the intention is to create a method that works in all wind conditions.

By comparison, the agreement scatter plot between the horizontal wind speeds measured by the sonic anemometer and the cup anemometer (as described in section 2.1, this is placed 4m higher) are presented for the entire month of June 2018 in Figure 16. This overlaps with three of the scanning pattern tests, see Table 2. A bias of 0.032 m/s and a scatter of 0.397 m/s is seen.

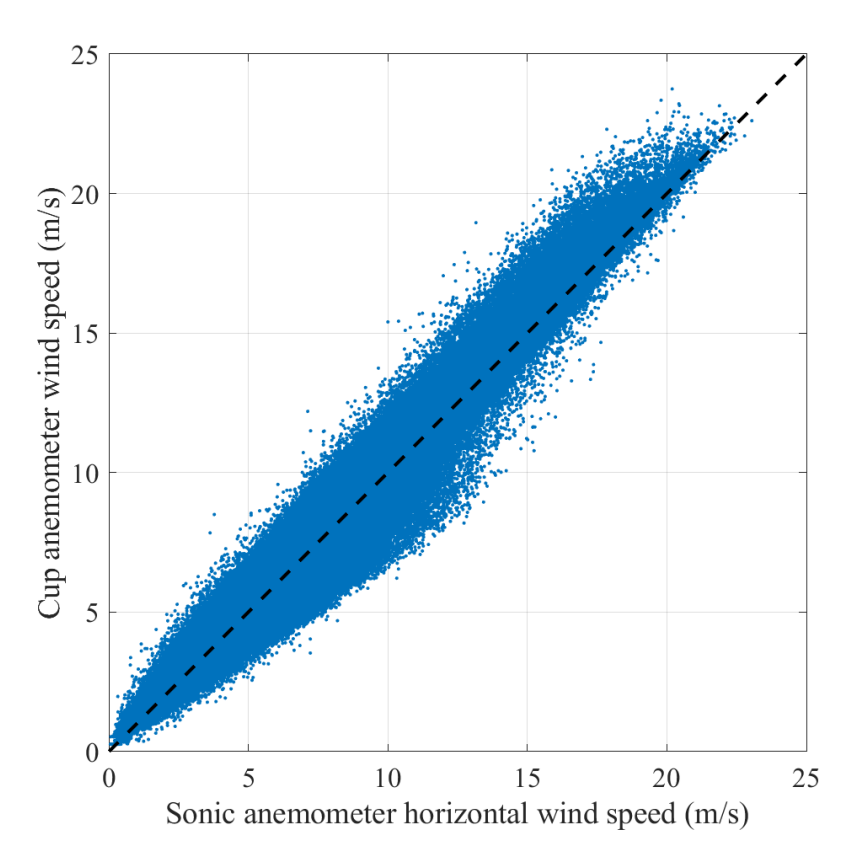


Figure 16 Scatter plot of horizontal wind speeds measured by the cup anemometer versus the sonic anemometer.

These statistics compare well with the results from the most accurate – slow-narrow – scanning pattern. It is clear that the wider azimuthal range introduces additional uncertainty in the reconstruction of a wind speed at a point. However, it is not certain from this experimental data set whether uncertainty introduced into the individual measurements by the very fast scanning patterns is a problem. The

statistical methods should theoretically be able to separate out noise from signal efficiently when there is sufficient data of even low quality.

Inspection of the close-up plots in section 4 indicates smoothed wind conditions in time – it appears that no matter what scanning pattern is used, turbulence with a scale below 10 seconds is unlikely to be resolved. For comparison, with the static WindCube v2, turbulent features down to about 3 seconds were observed. This may be caused by the characteristics of the Lidar scanning pattern, or the Gaussian Process analysis, or a combination of both.

In the results plots, it can be seen that certain (regularly-occurring) times have large errors. This is partly due to an error in the coding of the analysis, causing data before hour-breaks not to be used. Partly it is due to the Lidar switching itself off every 22:00 and then apparently recording incorrect data for a few seconds after switching on again.

Finally, it should be noted that this study has not resolved the question of the Cyclops effect. Prototype algorithms have been created to infer the wind velocity from beam speeds output from the Virtual Lidar at various locations at the same instant in time (as suggested in [2]). However, time has prevented conclusive investigation of this during this project (which was in any case not one of the objectives).

6 References

- [1] Stock-Williams C., "Gaussian Process Regression for Wind Field Reconstruction from Lidar" (2017) ECN-X--17-128
- [2] Stock-Williams C., Mazoyer P., Combrexelle S., "Wind field reconstruction from lidar measurements at high frequency using machine learning" (2018) J. Phys. Conf. Ser. 1102 012003
- [3] https://www.leosphere.com/products/scanning-wincube/
- [4] Bergman G., "Meteorological Mast 6 at EWTW Instrumentation Report" (2017) ECN-X--17-048
- [5] http://metek.de/product/usonic-3-scientific/ [Accessed 23 December 2018]